Article:

Frost, William James orcid.org/0000-0001-5249-1006, Seki, Takeshi, Kubota, Takahide et al. (4 more authors) (2021) Evaluation of Edge Domains in Giant Magnetoresistive Junctions. Applied Physics Letters. 172405. ISSN 0003-6951

https://doi.org/10.1063/5.0049315

Evaluation of Edge Domains in Giant Magnetoresistive Junctions

William Frost,[1, a)] Takeshi Seki,[2, 3] Takahide Kubota,[2, 3] Rafael Ramos,[4, b)] Eiji Saitoh,[5, 2, 4, 6, 7] Koki Takanashi,[2, 3, 8] and Atsufumi Hirohata[1, c)]

[1)] *Department of Electronic Engineering, University of York, Heslington, YO10 5DD, United Kingdom*
[2)] *Institute for Materials Research, Tohoku University, Sendai 980-8577, Japan*
[3)] *Center for Spintronics Research Network, Tohoku University, Sendai 980-8577, Japan*
[4)] *WPI Advanced Institute for Materials Research, Tohoku University, Sendai 980-8577, Japan*
[5)] *Department of Applied Physics, University of Tokyo, Tokyo 113-8656, Japan*
[6)] *Advanced Science Research Center, Japan Atomic Energy Agency, Tokai 319-1195, Japan*
[7)] *Institute of AI and Beyond, University of Tokyo, Tokyo 113-8656, Japan*
[8)] *Center for Science and Innovation in Spintronics, Core Research Cluster, Tohoku University, Sendai 980-8577, Japan*

We demonstrate that the spin-Seebeck effect can be used to estimate the volume of edge domains formed in a giant magnetoresistive (GMR) device. The thermal gradient induced by Joule heating can be harnessed by the addition of a ferromagnetically insulating channel of Fe_2O_3 on the sides of the GMR pillar. This generates a spin wave in the Fe_2O_3 which couples with the free-layer edge magnetisation and controls the reversal of the ferromagnetic layers in one direction only, increasing current density from $(1.1 \pm 0.1) \times 10^7$ A/cm^2 to $(7.0 \pm 0.5) \times 10^7$ A/cm^2. By simple assumption, we estimate the effect of the edge domain on magnetisation reversal to be (10-15)% by spin-transfer torque.

Spintronics has been attracting intensive studies over the last decades[1] for efficient computing and sensing. In spintronics, the generation and manipulation of spin-polarised electrons and current control the efficiency. One method is to use thermal gradient[2]. Spin-caloritronic devices represent an excellent avenue to improve device performance, efficiency and running cost by exploiting the waste heat produced in all current-driven devices[3]. The thermal effects caused by Joule heating are ubiquitous in device operation and act as an unavoidable source of wasted power, as well as affecting device performance due to thermal effects. However, the generated thermal gradient in a current-driven device can be exploited by the spin-Seebeck[4], Peltier[5] and Nernst[6] effects, depending upon which device geometry is needed.

Ferromagnetic insulators (FMI) such as Fe_2O_3 or yttrium iron garnet (YIG) are extremely sensitive to these thermal gradients to exhibit strong spin-caloritronic effects when exposed to them[7,8,9,10]. A spin wave can be generated via the spin-Seebeck effect when a current is applied to a device containing a FMI due to the Joule heating mentioned above. Therefore by including a FMI in a current-driven device the thermal gradients can begin to be used as a source of spin-current.

If this spin-current can be introduced to the ferromagnetic layers of a magnetoresistive device then the switching behaviour can be manipulated. The generated spin wave should act as a secondary source of torque as current flows through the device. In turn, this should lower the required current density for magnetisation switching as the required torque remains unchanged. As such the efficiency of the device can be improved by harnessing the wasted energy that is usually detrimental to device performance.

FIG. 1: Device with the insulating AlO replaced by Fe_2O_3.

In this study a standard current-perpendicular-to-plane (CPP) giant magnetoresistance (GMR) device based on Heusler alloys has been modified to exhibit these effects. Heusler alloys have been used as they represent a family of materials with excellent potential for device application due to high values of saturation magnetisation and Curie temperature (M_S >1000 emu/cm^3 and T_C >900 K for Co_2FeSi) and the potential for 100% spin polarisation at the Fermi level. The standard insulator around the GMR pillars was replaced with Fe_2O_3 to act as a spin-wave source. This spin-wave generation controls the current density for switching and introduces a strong asymmetry due to the coercivity differences between the Heusler alloy layers and the FMI, allowing us to estimate the volume of the edge domains in a pillar.

An unconventional GMR pillar was fabricated, as shown in fig. 1. A typical Heusler-based GMR multilayer consisting of $Co_2Fe_{0.4}Mn_{0.6}Si$ (CFMS) (5)/$Ag_{0.78}Mg_{0.22}$ (5)/CFMS (5) was grown on a Cr (20)/Ag (40) seed layer on an MgO(001) substrate under ultrahigh vacuum via magnetron sputtering, where all thicknesses are given in nanometres. The Cr/Ag seed layer was used to remove island growth and to promote strong texture in the CFMS layer[11] and was acted as the bottom electrode of a CPP-GMR junction. A capping layer of Ag (2 nm)/Au (5 nm) was added. The seed and Heusler-alloy layers were annealed at 650 °C and 500 °C respectively to improve the interfacial smoothness and to promote crystallisation and ordering of the CFMS and the $Ag_{0.78}Mg_{0.22}$ layers[12].

Photo- and electron-beam lithography and Ar-ion milling were used to fabricate a series of elongated pillars with long axes from 100 nm to 800 nm, however as shown in fig. 1 the milling stopped 1 nm into the lower FM layer. The Fe_2O_3 was then deposited around the pillar in place of the usual AlO insulator. For adhesion, it was necessary to add a secondary

[a)] Present address: Oxford Instruments Plasma Technology, Bristol BS49 4AP, United Kingdom
[b)] Present address: Center for Research in Biological Chemistry and Molecular Materials, Universidade de Santiago de Compostela, 15782 Santiago de Compostela, Spain
[c)] Electronic mail: atsufumi.hirohata@york.ac.uk

FIG. 2: GMR curves for a pillar (120 and 60 nm in long and short axes, respectively) (a) with and (b) without Fe_2O_3 with a sensing current of 100 μA. Red and blue curves represent the field sweep from negative to positive and *vice versa* respectively. Note that the shape of the GMR curves are independent of the amplitude of the sensing current up to 1 mA

FIG. 3: Current switching profiles for the same device as shown in fig. 2(a) with applied fields of (a) -10 and (b) 75 Oe corresponding to the fields to form distinctive magnetic configurations as appeared in Fig. 2, where (b) has a current in the opposite direction. In (a), red, blue and green curves represent the current sweep from 0 to negative, from negative to positive and *vice versa* respectively, while in (b), that from 0 to positive, from positive to negative and *vice versa* respectively.

seed layer consisting of Cr (1 nm)/AlO (2 nm). Due to the lack of adhesion it was not possible to stably anneal Fe_2O_3. Therefore the crystallinity of the FMI channels is limited.

Device properties were measured using a HiSOL HMP400-SMS probe station with a Keithley 2400 sourcemeter and a Keithley 2182A nanovoltmeter, giving high resolution. Magnetisation reversal was induced using both field- and current-induced methods to analyse the effects of the FMI channels.

The fabricated GMR pillars were first evaluated in the standard manner using an applied external field. Figure 2(a) shows the magnetoresistance trace for a pillar with Fe_2O_3 present, which was initially saturated by the negative field, fixing the Fe_2O_3 moment as shown in fig. 2(a). It is immediately obvious that there is a significant asymmetry in the signals between a positive-to-negative and a negative-to-positive field sweep, with the difference in MR between the parallel and antiparallel states (ΔMR) values of $(32.8 \pm 0.1)\%$ and $(10.2 \pm 0.1)\%$ respectively. Furthermore there is a large difference between the field values of the peak GMR value, decreasing from (70 ± 2) Oe to (-18 ± 2) Oe when the ΔMR increases. The switching field for nucleated reversal after magnetisation rotation, *i.e.*, the sharp change following the sloped parts, changes similarly from (126 ± 2) Oe to (-54 ± 2) Oe. These differences are reproducible and independent of the order of the sweep directions.

The decrease in the switching field can be attributed to the formation of edge domains (partially antiparallel state), whose magnetisations are coupled to the magnetic moments in the Fe_2O_3 surrounding layer. These edge domains can be easily rotated by a small change in the applied field, making the antiparallel state to be unstable as seen in the figure. Since the coercivity of Fe_2O_3 is greater than the coercivity of the GMR pillars, the edge domains can only be fully aligned in one direction of the magnetisation during the reversal as schematically shown in fig. 2(a).

The reduction in the value of the magnetoresistance is also due to the direct coupling between the layers in the stack and the edge of the pillar coupled with Fe_2O_3, where edge domains form. Since there is no reversal in the magnetisation of Fe_2O_3 within the fields applied to achieve the magnetisation reversal in the CFMS layers, there has to be a region of transient magnetisation at the interface between the Heusler-alloy layers and $Fe_2O_3$where the ferromagnetic exchange coupling must be accounted for. The two magnetisations cannot be in direct opposition when in direct contact. This creates regions of spin which are not collinear with the device orientation and as such do not contribute to the GMR signal. They also aid the reversal of the free layer and such a reduced coercivity is observed.

Additionally this coupling is responsible for the shape of the positive-to-negative sweep, where a kink is observed in the blue curve at 50 Oe in fig. 2(a). This is at the same positive field value as the coercivity in the negative-to-positive direction, implying that a magnetisation change is occurring not due to the external field but due to the coupling. This is why there is a dramatic change in shape around this point where the magnetisation reversal changes from being dominated by the coupling to controlled by the external field.

Figure 2(b) is measured in the same manner as fig. 2(a) but for a reference device without Fe_2O_3, insulated by pure AlO. The trace is far more symmetric than for fig. 2(a), with no field direction dependence to the signal. The coercivity values for the antiparallel-to-parallel switch are (96 ± 2) Oe and (-92 ± 2) Oe in the negative-to-positive and positive-to-negative field directions respectively. The peak GMR values are $(21.7 \pm 0.2)\%$ and $(22.7 \pm 0.3)\%$ at field values of (74 ± 2) Oe and (-65 ± 2) Oe, comparable to the positive-to-negative field sweep in fig. 2(a). This is consistent with a lack of exchange coupling from Fe_2O_3.

Figure 3 shows the current-driven reproducible switching behaviour for the same device as shown in fig. 2(a). Figure 3(a) shows the switching behaviour starting from the fully antiparallel state as achieved at -10 Oe in fig. 2(a) in the positive-to-negative field sweep as you approach the peak of the switching at (-18 ± 2) Oe. A negative current (applied top to bottom) reverses the magnetisation of the free layer by spin-transfer torque (STT) resulting in a gradual reduction in resistance. The switching current density, j_{sw}, is estimated to be $(8.0 \pm 0.7) \times 10^7$ A/cm^2. The value is the threshold for a final transition after significant rotation of the magnetisation, shown via the extensive curvature in the GMR curves in both field- and current-driven switching systems. Here we consider three contributions for the magnetisation switching, (i) conventional STT by the pinned layer, (ii) the influence of the edge domains exchange-coupled with a spin wave generated in Fe_2O_3 and (iii) Joule heating.

As observed without Fe_2O_3, a negligible asymmetry is measured in the GMR curves from negative to positive saturation and *vice versa*. However, with Fe_2O_3, a prominent asymmetry is measured as seen in fig. 2(a), which contains the above explained edge magnetic domains coupled to the spin wave (ii) generated in Fe_2O_3 by the thermal gradient al-

FIG. 4: Current switching profiles for a similar device as shown in fig. 2(b) with field of 3 Oe corresponding to the fields to form the initial antiparallel configuration as appeared in fig. 2.

most perpendicular to the plane. Therefore the current-driven switching must be affected by Fe_2O_3 around the edge of the free layer, which are aligned parallel to the pinned layer by the initial application of the negative field as described above and therefore will produce two contributions (i) and (ii) as schematically shown in the figure. The STT (i) switches a central region of the magnetisation of the free layer, while those in the edge domain are maintained by (ii), forming the partially antiparallel state. It is therefore possible for the magnetisation to be reversed using a negative current from antiparallel to parallel states. Removal of the applied current does not reorient the free layer but the minor increase in the resistance suggests the decrease in the volume of the edge domains (ii) in addition to the Joule heating by the current (iii). It should be noted that the magnetisation switching from the parallel to antiparallel state cannot be achieved by a current up to 40 mA, which indicates that STT (i) may not be strong enough for switching although some minor increase and instability in resistance can be seen in the positive current in the figure.

Figure 3(b) shows the same process in the opposite field orientation starting from the partially antiparallel state as achieved at 75 Oe in fig. 2(a). Here j_{sw} has a value of $(7.0 \pm 0.5) \times 10^7$ A/cm^2 controlled by the competition between the the three contributions (i)-(iii). First, a reduction in the resistance at very low currents is observed, which can be associated with gradual magnetisation rotation in the minor domains formed between the central region and the edge domains in the free layer as shown in grey in fig. 3(b). This may possibly due to STT through the central domain to instabilise the minor domains (i) and the exchange coupling induced by the outer edge domains. A metastable state is then reached as the edge domains (ii) and Joule heating (iii) are not strong to reverse the magnetisation in the central region of the free layer up to j_{sw} as the partial antiparallel configuration is stable from the viewpoint of the STT (i). Above j_{sw}, spin-torque oscillation may start to occur as reported in a similar system[13], which makes the magnetisation of the central region to be unstable and assists the magnetisation reversal by the processes (ii) and (iii). This may lead to the significant instability of the device resistance at high currents. It is also possible that the instability is due to the lack of total crystallinity in Fe_2O_3 without annealing, local spin waves may be generated, which in turn perturb the magnetisation in the edge domains of the free layer, causing variations in the resistance. Additional imperfections from diffusion or intermixing in Fe_2O_3 may create pinholes in Fe_2O_3 which further change local spin-wave environments.

Figure 4 shows the current switching data by the conventional STT (i) in a similar device without Fe_2O_3 as shown in fig. 2(b). It is clear that the antiparallel state is more uniform in this device with two distinct plateaus separated by sharp switching. The switching current densities are lower than for the case above with values of j_{sw} of $(1.1 \pm 0.1) \times 10^7$ A/cm^2 and $(2.2 \pm 0.2) \times 10^7$ A/cm^2 for the negative and positive currents respectively. The increased stability is due to the removal of the influence of Fe_2O_3 no longer forming the edge/minor domains. The reversal is simply controlled by a nucleation event, most likely at an edge where damage from milling has occurred as similarly observed in our earlier studies without Fe_2O_3[12,14]. The difference in j_{sw} confirms the magnetic stability of the edge domains induced by Fe_2O_3 in fig. 3, which may not be ideal for fast and coherent magnetisation reversal for device applications. It is therefore important to estimate the volume of the edge domains.

These results indicate that the presence of the spin wave in Fe_2O_3 can assist the magnetisation reversal only when the spin-wave generated in Fe_2O_3 is in parallel with the magnetisation of the free layer as discussed above, however, the edge/minor domains magnetically coupled to Fe_2O_3 are found to further increase j_{sw}. The presence of Fe_2O_3, which has non-ideal crystallinity, may induce strong pinning sites at the interface with the Heusler-alloy layer inducing a significant rotational component to the magnetisation reversal. Since the rotational components account for $10-15\%$ of the total resistance change, the edge domain volume can be estimated as this proportion of the free layer as compared with the central region consisting of approximately a half of the volume switched at j_{sw} in fig. 3, leaving the remaining almost 1/3 of the volume to from minor domains between them. Such estimation can be complementary to the conventional activation volume analysis for the magnetisation reversal[15] and suggests the elimination of such minor domains can reduce j_{sw}.

Furthermore the presence of any disorders or dislocations will reduce the spin polarisation of the Heusler-alloy layer. If the spin polarisation of the pinned layer is reduced, the associated STT is reduced and j_{sw} is increased. Therefore improvements are needed to the fabrication of the pillars with Fe_2O_3, especially the improvement of the crystallinity of Fe_2O_3, in order to realise the potential to effectively take advantage of thermally-induced spin waves.

In summary, we have shown that a FMI in contact with the edge of a GMR device can heavily influence its behaviour. Significant asymmetry is induced in the current-induced magnetisation switching depending upon the relative magnetisation of the FMI and the free layer due to the thermal gradients from Joule heating, which in turn create spin waves in the device coupling with the edge domains in the free layer. This may also create different field dependent behaviour. This is useful for determination of the volume of edge domains and for the evaluation of the nature of coupling between FMI and GMR structures. Control of GMR devices for niche application or asymmetric reversal may be possible using FMI edge channels.

This work was partially supported by EPSRC-JSPS Core-to-Core Programme (EP/M02458X/1), JST CREST (No. JPMJCR17J5), Global Institute for Materials Research Tohoku (GIMRT), Institute of AI and Beyond of the University of Tokyo, JST ERATO "Spin Quantum Rectification Project" (No. JPMJER1402) and JSPS Grant-in-Aid for Scientific Research (S) (No. JP19H05600) and (C) (No. JP20K05297 and JP20K05296). R.R. acknowledges support from the European Commission (734187-SPICOLOST, H2020-MSCA-RISE-2016), Marie Sklodowska-Curie Action SPEC (No 894006) and the Spanish Ministry of Science.

All data are available on the dedicated database of the University of York.

[1] A. Hirohata, K. Yamada, Y. Nakatani, I.-L. Prejbeanu, B. Diény, P. Pirro, B. Hillebrands, Review on spintronics: Principles and device applications, Journal of Magnetism and Magnetic Materials 509 (2020) 166711.

[2] G. Bauer, E. Saitoh, B. J. van Wees, Spin caloritronics, Nature Materials 11 (2012) 391.

[3] M. Mizuguchi, S. Nakatsuhi, Energy-harvesting materials based on the anomalous Nernst effect, Science and Technology of Advanced Materials 20 (2019) 262–275.

[4] K. Uchida, S. Takahashi, K. Harii, J. Ieda, W. Koshibae, K. Ando, S. Maekawa, E. Saitoh, Observation of the spin Seebeck effect, Nature 455 (2008) 778–781.

[5] J. Flipse, F. K. Dejene, D. Wagenaar, G. E. Bauer, J. B. Youssef, B. J. Van Wees, Observation of the spin peltier effect for magnetic insulators, Physical Review Letters 113 (2014) 027601.

[6] S. Meyer, Y. T. Chen, S. Wimmer, M. Althammer, T. Wimmer, R. Schlitz, S. Geprags, H. Huebl, D. Kodderitzsch, H. Ebert, G. E. Bauer, R. Gross, S. T. Goennenwein, Observation of the spin Nernst effect, Nature Materials 16 (2017) 97–981.

[7] H. Chang, P. A. Praveen Janantha, J. Ding, T. Liu, K. Cline, J. N. Gelfand, W. Li, M. C. Marconi, M. Wu, Role of damping in spin Seebeck effect in yttrium iron garnet thin films, Science Advances 3 (2017) e1601614.

[8] P. Jiménez-Cavero, I. Lucas, A. Anadón, R. Ramos, T. Niizeki, M. H. Aguirre, P. A. Algarabel, K. Uchida, M. R. Ibarra, E. Saitoh, L. Morellón, Spin Seebeck effect in insulating epitaxial *gamma*-Fe_2O_3 thin films, Applied Physics Letters Materials 5 (2017) 026103.

[9] L. Baldrati, C. Schneider, T. Niizeki, R. Ramos, J. Cramer, A. Ross, E. Saitoh, M. Kläui, Spin transport in multilayer systems with fully epitaxial NiO thin films, Physical Review B 98 (2018) 014409.

[10] R. Lebrun, A. Ross, S. A. Bender, A. Qaiumzadeh, L. Baldrati, J. Cramer, A. Brataas, R. A. Duine, M. Kläui, Tunable long-distance spin transport in a crystalline antiferromagnetic iron oxide, Nature 561 (2018) 7722.

[11] J. Sagar, L. R. Fleet, A. Hirohata, K. O'Grady, Activation volumes in Co_2FeSi thin films, IEEE Transactions on Magnetics 47 (2011) 2440–2443.

[12] T. Kubota, Y. Ina, Z. Wen, H. Narisawa, K. Takanashi, Current perpendicular-to-plane giant magnetoresistance using an $L1_2$ Ag_3Mg spacer and $Co_2Fe_{0.4}Mn_{0.6}Si$ Heusler alloy electrodes: Spacer thickness and annealing temperature dependence, Physical Review Materials 1 (2017) 044402.

[13] T. Seki, T. Kubota, T. Yamamoto, K. Takanashi, Size dependence of vortex-type spin torque oscillation in a Co2Fe0.4Mn0.6Si Heusler alloy disk, Journal of Physics D: Applied Physics 51 (2018) 075005.

[14] T. Kubota, Z. Wen, K. Takanashi, Current-perpendicular-to-plane giant magnetoresistance effects using Heusler alloys, Journal of Magnetism and Magnetic Materials 492 (2019) 165667.

[15] J. Sagar, H. Sukegawa, L. Lari, V. K. Lazarov, S. Mitani, K. O'Grady, A. Hirohata, The effect of interfaces on magnetic activation volumes in single crystal Co_2FeSi Heusler alloy thin films, Applied Physics Letters 101 (2012) 102410.

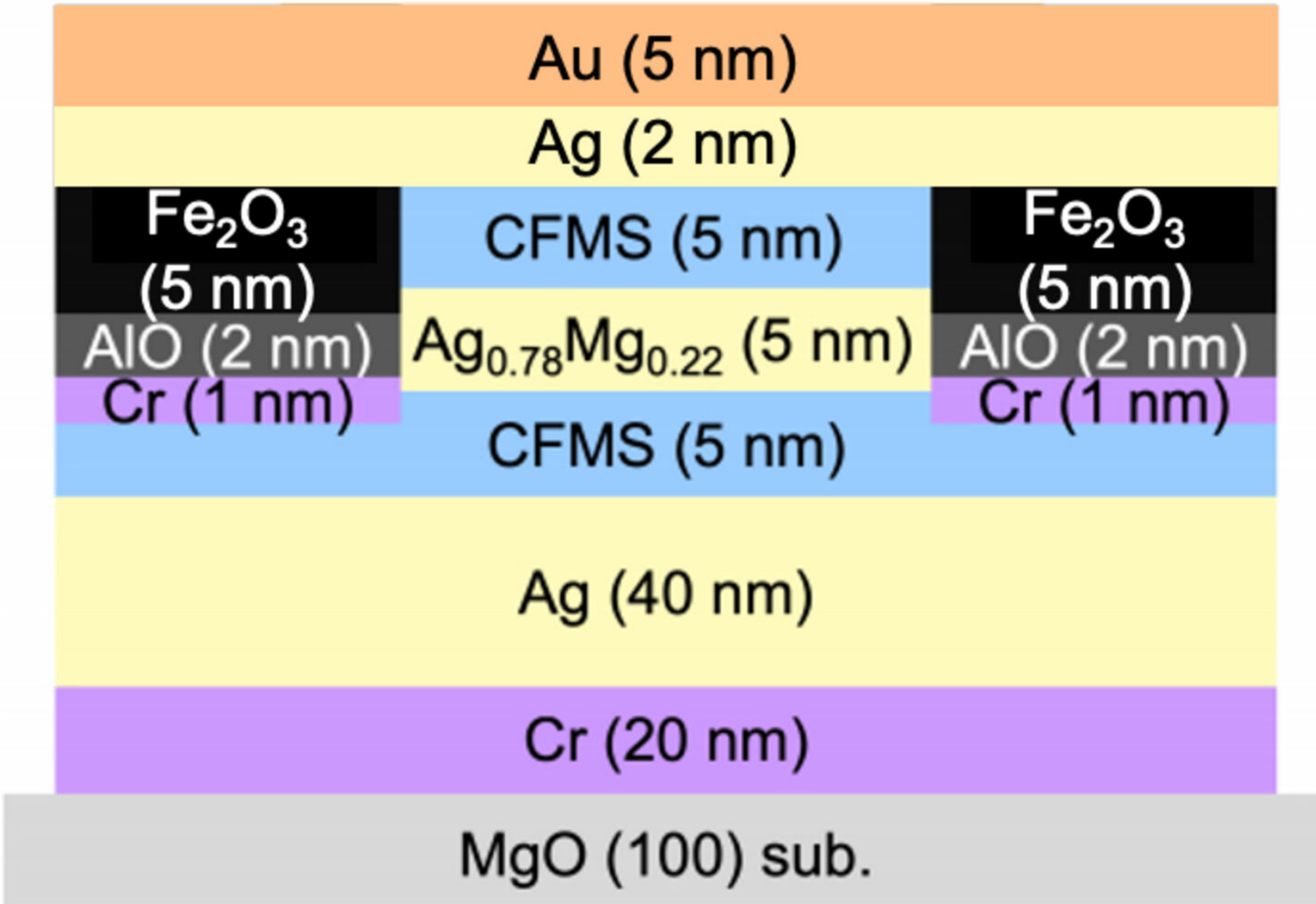

Au (5 nm)
Ag (2 nm)
Fe_2O_3 (5 nm)
CFMS (5 nm)
Fe_2O_3 (5 nm)
AlO (2 nm)
$Ag_{0.78}Mg_{0.22}$ (5 nm)
AlO (2 nm)
Cr (1 nm)
Cr (1 nm)
CFMS (5 nm)
Ag (40 nm)
Cr (20 nm)
MgO (100) sub.

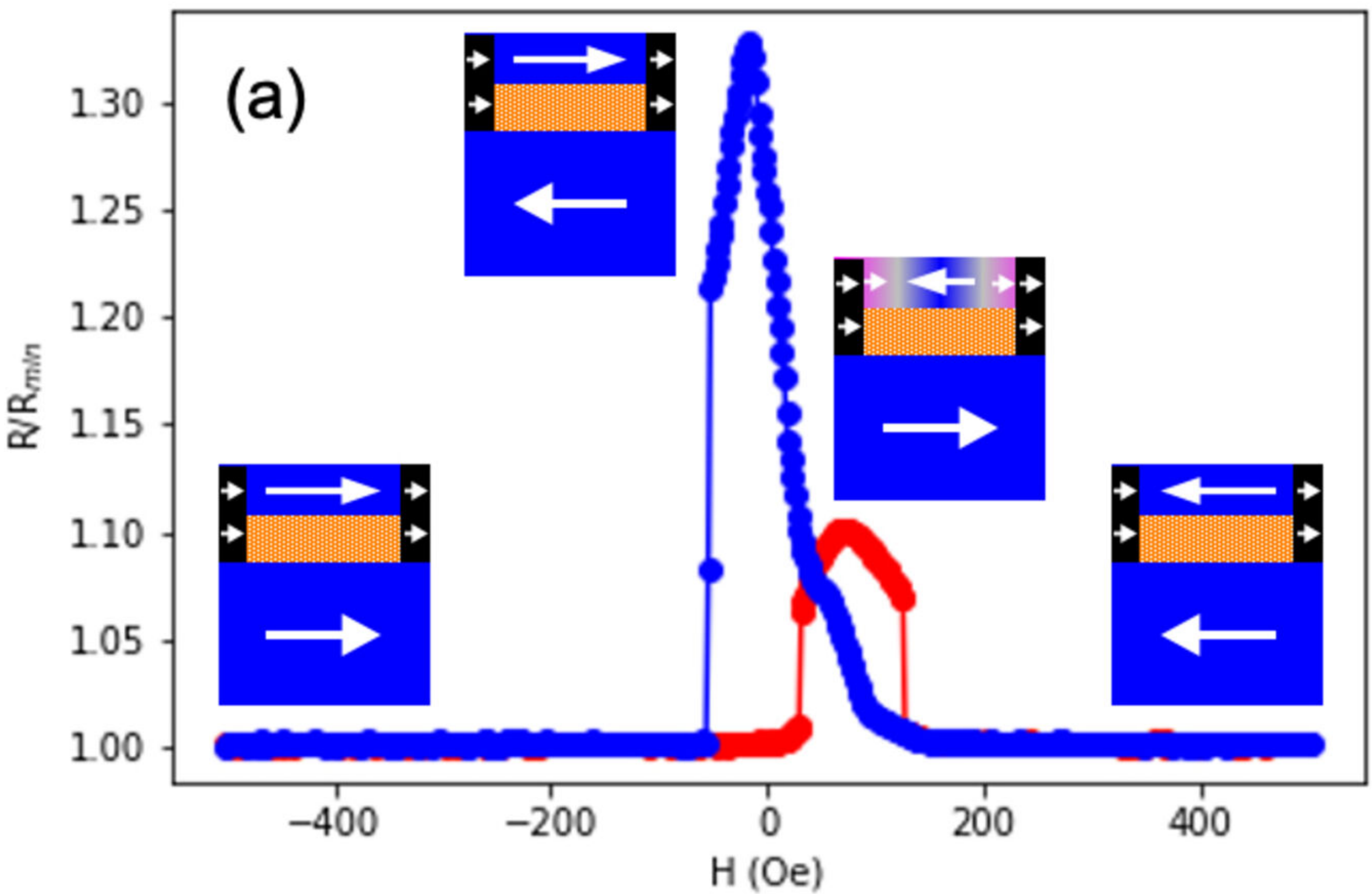
(a)
1.30
1.25
1.20
1.15
1.10
1.05
1.00
R/R_min
−400
−200
0
200
400
H (Oe)

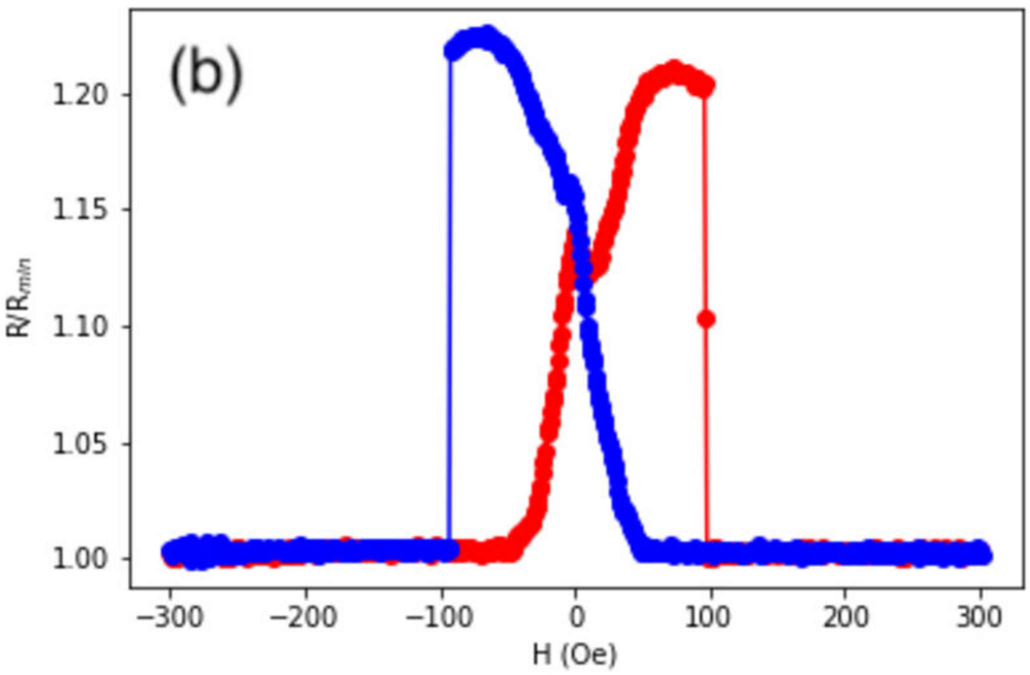

(b)
1.20
1.15
1.10
1.05
1.00
R/R$_{min}$
−300
−200
−100
0
100
200
300
H (Oe)

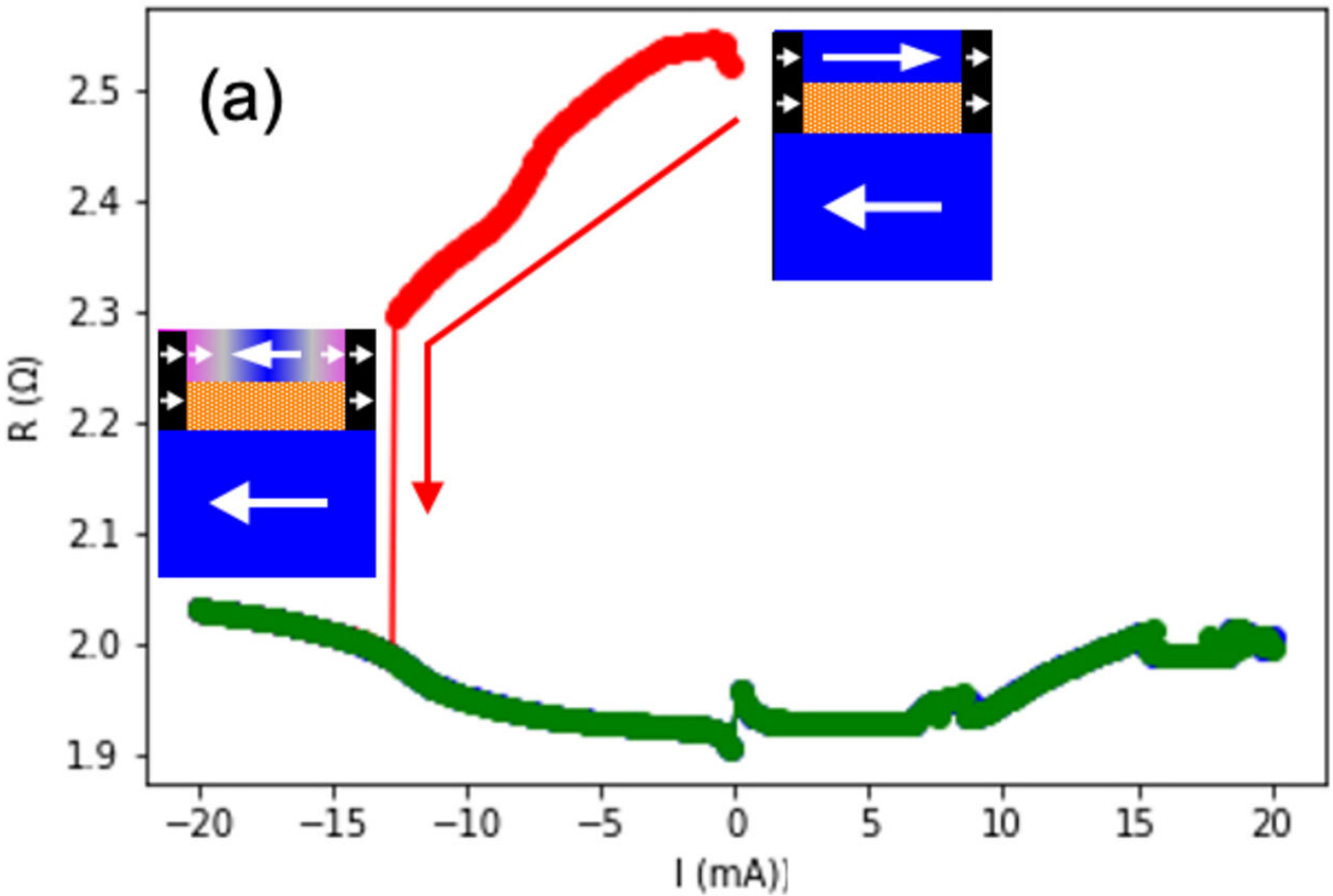
(a)
2.5
2.4
2.3
2.2
2.1
2.0
1.9
R (Ω)
−20
−15
−10
−5
0
5
10
15
20
I (mA)

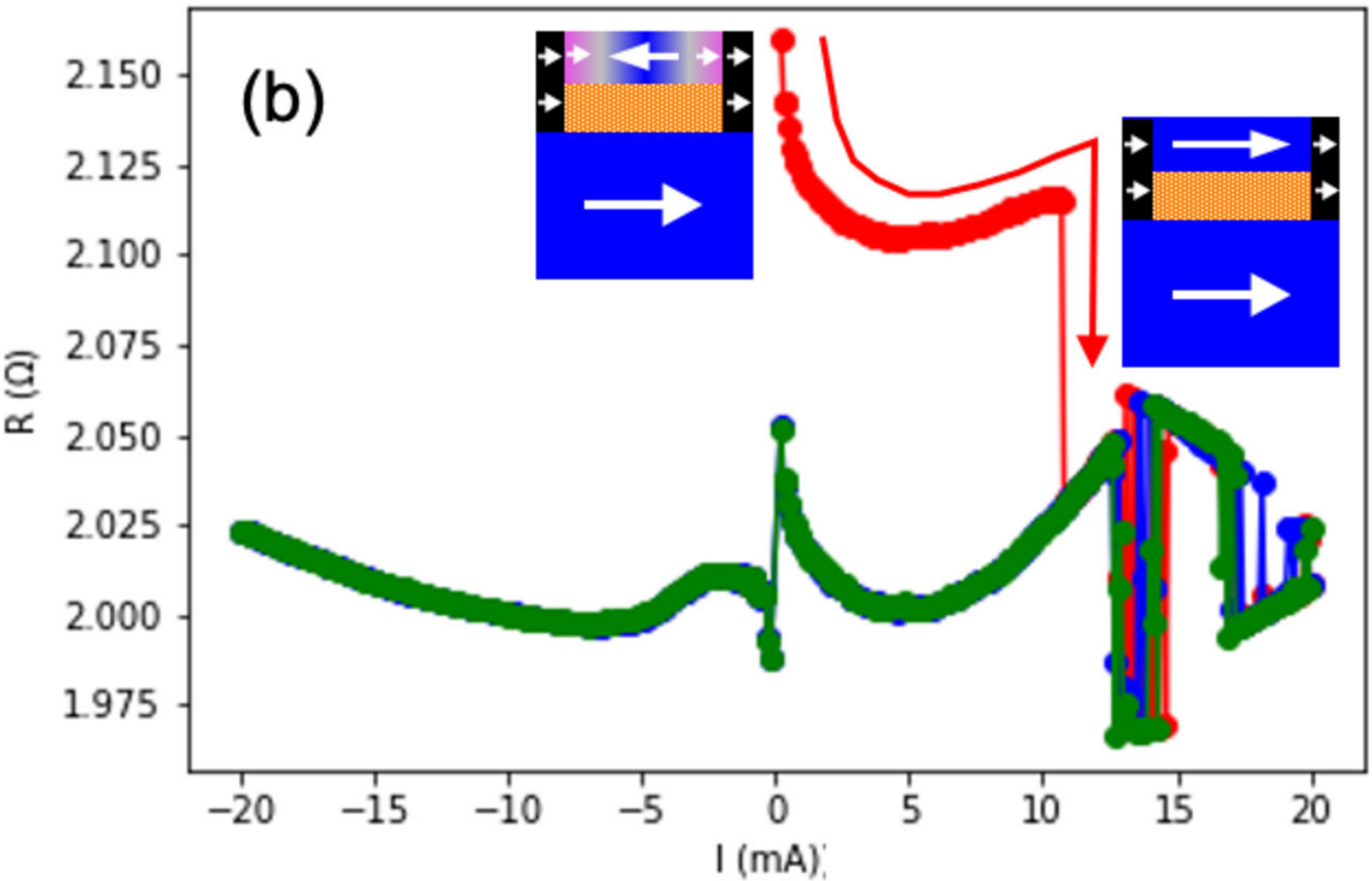
(b)
R (Ω)
2.150
2.125
2.100
2.075
2.050
2.025
2.000
1.975
−20
−15
−10
−5
0
5
10
15
20
I (mA)

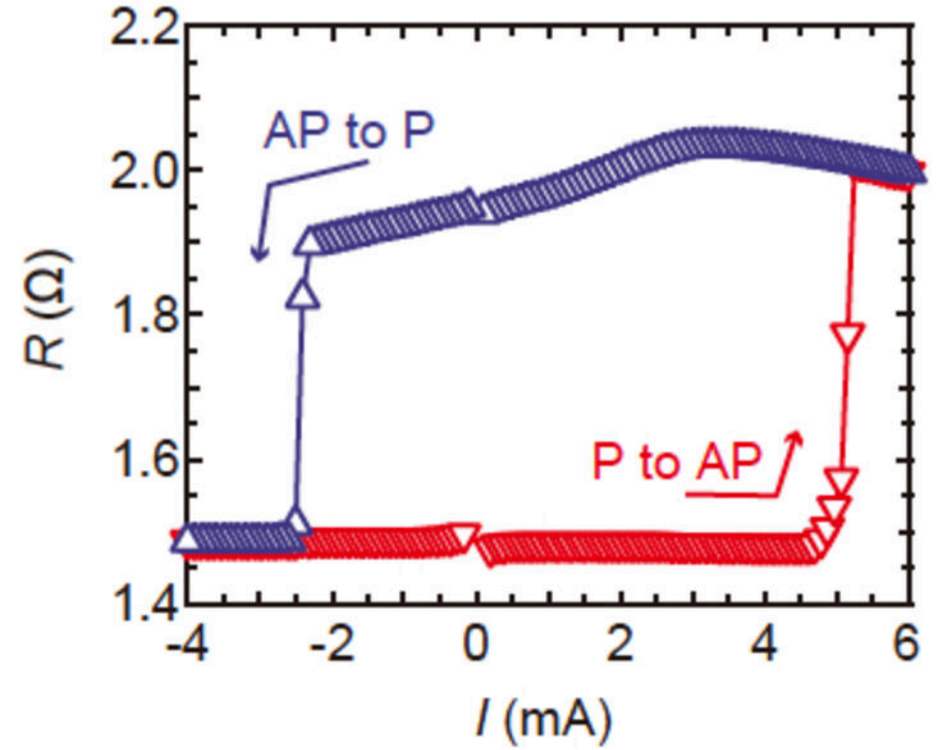

AP to P
P to AP
2.2
2.0
1.8
1.6
1.4
R (Ω)
-4
-2
0
2
4
6
I (mA)